Vibrational Relaxation Pathways of AI and AII Modes in *N*-Methylacetamide Clusters

L. Piatkowski* and H. J. Bakker

FOM Istitute for Atomic and Molecular Physics, Science Park 104, 1098 XG Amsterdam, The Netherlands

Received: August 11, 2010; Revised Manuscript Received: September 17, 2010

We studied the pathways of vibrational energy relaxation of the amide I ($\sim$1660 cm^{-1}) and amide II ($\sim$1560 cm^{-1}) vibrational modes of *N*-methylacetamide (NMA) in CCl_4 solution using two-color femtosecond vibrational spectroscopy. We measured the transient spectral dynamics upon excitation of each of these amide modes. The results show that there is no energy transfer between the amide I (AI) and amide II (AII) modes. Instead we find that the vibrational energy is transferred on a picosecond time scale to a common combination tone of lower-frequency modes. By use of polarization-resolved femtosecond pump−probe measurements we also study the reorientation dynamics of the NMA molecules and the relative angle between the transition dipole moments of the AI and AII vibrations. The spectral dynamics at later times after the excitation (>40 ps) reveal the presence of a dissociation process of the NMA aggregates, trimers, and higher order structures into dimers and monomers. By measuring the dissociation kinetics at different temperatures, we determined the activation energy of this dissociation $E_a = 35 \pm 3$ kJ mol^{-1}.

Introduction

The function of proteins is intimately related to their spatial structure and conformational dynamics. Any deviations of the functional structure, e.g., as a result of errors occurring during the folding process, can lead to disastrous consequences. For instance it has been shown that errors in the structure of particular proteins can cause diseases like Alzhemeir's and Parkinson's.[1] The structure and conformational dynamics of proteins and polypeptides are closely connected to the dynamics of their intra- and intermolecular hydrogen bonds. The hydrogen bonds act to stabilize the conformation and also play an essential role in the energy dynamics of the protein.

To obtain molecular-scale insight into the hydrogen-bond dynamics of complex systems like proteins, it is often advantageous to study simpler molecular systems that form good model systems for these dynamics. An essential element of the structure of proteins is their backbone that consists of linked amide (−CO-NH−) groups. *N*-Methylacetamide (NMA) is the simplest molecule containing the amide motif, and a study of the hydrogen-bond interactions of NMA can thus give insight in the hydrogen-bond interactions of protein backbones.

The properties of NMA and NMA aggregates have been extensively studied with different experimental and theoretical methods such as infrared spectroscopy,[2−8] dielectric spectroscopy[9,10] and molecular simulations.[11−17] These studies addressed different properties of NMA such as its thermodynamical properties[2,3,11,12] and its vibrational energy dynamics and couplings.[6,8,14,15] In spite of its apparent chemical simplicity, NMA is quite complex in terms of its vibrational spectrum that contains no less than seven different amide vibrational bands.[3,4,14,18] These amide vibrations (residing between $\sim$400 and $\sim$1720 cm^{-1}), the fundamentals, and combination tones form a dense manifold of vibrational states. In case the NMA molecules are hydrogen bonded, the vibrational spectrum becomes even more complex, as each intramolecular state becomes dressed with excitations and de-excitations in the coupled intermolecular hydrogen-bond modes.

The reported vibrational studies addressed the properties of NMA−water systems. So far no results have been reported on the vibrational properties of NMA-NMA aggregate structures, although NMA aggregates constitute a nice model system for proteins that fold as a result of hydrogen-bond formation between the different amide groups of the protein backbone. Here we report on a polarization-resolved two-color femtosecond spectroscopic study of the vibrational dynamics of hydrogen-bonded NMA aggregates. We study the probability of energy transfer between the different amide modes of the NMA molecules and the vibrational energy relaxation pathways. We also study the kinetics of the formation and breaking of hydrogen bonds of NMA aggregates.

Experimental Section

The polarization-resolved two-dimensional experiment employs femtosecond mid-infrared pulses. These pulses are generated by frequency conversion processes that are pumped with the near-infrared 800-nm pulses derived from a high energy Ti:Sapphire amplifier system. This system is a coherent "Legend Duo" regenerative amplifier that delivers 40-fs pulses with a pulse energy of 7 mJ per pulse at a repetition rate of 1 kHz. We use about 6 mJ to pump an optical parametric amplifier (HE-TOPAS). The produced signal and idler pulses are used in a difference frequency mixing process in a silver gallium disulfide ($AgGaS_2$) crystal resulting in 60 μJ pulses with a central wavelength of $\sim$6000 nm ($\sim$1650 cm^{-1}), a pulse duration of $\sim$55 fs, and a spectral bandwidth of $\sim$400 cm^{-1}.

In the experiment the AI or AII mode is excited with a relatively narrow band pump pulse and the transient changes in absorption resulting from this excitation are monitored with a second broadband IR pulse. The narrow-band pump pulse is obtained by spectrally filtering the generated broadband infrared pump spectrum (Figure 1) with a home-built Fabry−Perot filter. This filter is an air-spaced cavity that is created by two closely spaced parallel semitransparent windows (reflectivity $R = 90\%$). The Fabry−Perot filter transmits only the wavelengths that constructively interfere in exit channel of the cavity. By changing the distance between the two windows we can tune

* To whom correspondence should be addressed E-mail: l.piatkowski@amolf.nl.

10.1021/jp107590b
Published on Web 10/13/2010

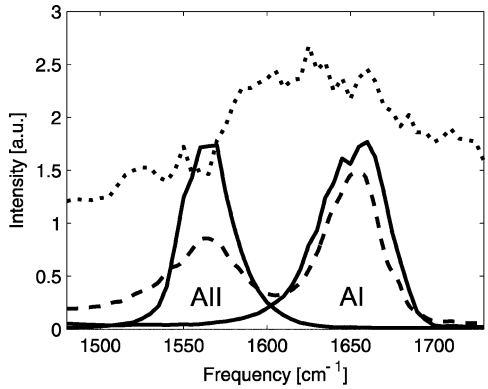

Figure 1. Experimental spectra of the probe pulse (dotted) and two pump spectra when pumping either the amide I or amide II vibration of NMA in CCl_4 solution (solid lines). The dashed line represents the absorption spectrum of a solution of 5 M.

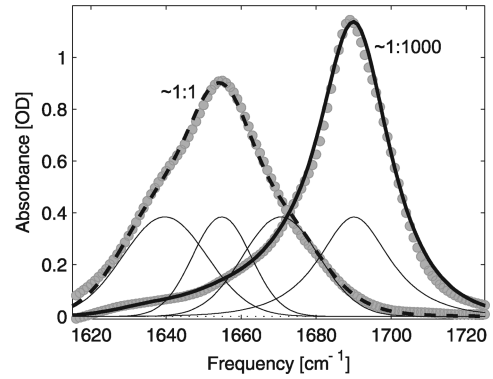

Figure 2. Linear spectra of a 10 mM and a 5 M solution of NMA in CCl_4. The gray circles represent the data points, and the thick solid (10 mM) and dashed (5 M) lines are the result of a global fit. The thin lines represent the four sub-bands used to describe the linear spectra at all concentrations.

the transmitted beam wavelength and the bandwidth. The spectral bandwidth of the pump pulses used in the experiments is 40−50 cm^{-1}.

We measure the pump-induced frequency-resolved transient absorption spectra ($\Delta\alpha$) as a function of time delay between the narrow-band pump and broadband probe pulses. The pump pulse excites the NMA molecules from the equilibrium ground state $v = 0$ to the first excited state, $v = 1$ of the AI or AII mode. This excitation is observed as a bleach and stimulated emission at frequencies matching the $v = 0 \rightarrow 1$ transition and an induced absorption at frequencies matching the $v = 1 \rightarrow 2$ transition. The probe and reference beams are split off from the broadband infrared pulse beam using two wedged BaF_2 windows. The probe is sent into a 4-fs resolution delay stage. The pump and probe pulses are focused to the same spot in the sample using a gold-coated parabolic mirror. The reference pulse is also focused in the sample by the same mirror but not in overlap with the pump. After the sample, the probe and reference beams are dispersed with an Oriel monochromator and detected with an Infrared Associates 2 × 32 pixels mercury−cadmium-telluride (MCT) detector array. The reference allows for a frequency-resolved correction for shot-to-shot fluctuations of the probe−pulse energy.

Before entering the sample, the polarization of the probe is rotated at 45° with respect to the polarization of the narrow-band pump using a wire-grid polarizer. After the sample the polarization component parallel to the pump or the component perpendicular to the pump is selected using a polarizer mounted in a motorized rotation stage. The thus obtained transient absorption changes $\Delta\alpha_{\parallel}(t, \nu)$ and $\Delta\alpha_{\perp}(t, \nu)$ are used to construct the so-called isotropic signal

$$\Delta\alpha_{iso}(t, \nu) = \frac{\Delta\alpha_{\parallel}(t, \nu) + 2\Delta\alpha_{\perp}(t, \nu)}{3} \quad (1)$$

The isotropic signal $\Delta\alpha_{iso}(t, \nu)$ is not sensitive to depolarization of the excitation and gives information on the rate of vibrational energy relaxation and energy transfer.

The signals $\Delta\alpha_{\parallel}(t, \nu)$ and $\Delta\alpha_{\perp}(t, \nu)$ are also used to construct the so-called anisotropy parameter $R(t, \nu)$ that exclusively represents the dynamics of the depolarization of the excitation

$$R(t, \nu) = \frac{\Delta\alpha_{\parallel}(t, \nu) - \Delta\alpha_{\perp}(t, \nu)}{3\Delta\alpha_{iso}(t, \nu)} \quad (2)$$

The anisotropy parameter $R(t, \nu)$ represents the normalized difference between parallel and perpendicular pump−probe polarizations. $R(t, \nu)$ is proportional to the second-order auto-correlation function of the direction of the transition dipole moment.[19]

The samples are formed by solutions of NMA in CCl_4. We study these solutions at 7 different concentrations: 5 M (molecular ratio NMA−CCl_4 1:1), 0.5 M (1:20), 0.2 M (1:50), 0.1 M (1:100), 50 mM (1:200), 30 mM (1:330), and 10 mM (1:1000). In the study of the vibrational dynamics of the NMA aggregates we used a highly concentrated sample of 5 M of NMA in CCl_4 (see Figure 2). The samples were placed between two 2 mm thick CaF_2 windows separated by Teflon spacers with thicknesses ranging from 5 μm to 1.2 mm. For the experiments at elevated temperatures we have used a home-built sample cell in which the heat source is formed by resistors surrounding the sample. The temperature of the sample was monitored with a temperature probe attached directly to the surface of one of the CaF_2 windows. During the experiments the experimental setup was constantly flushed with N_2 gas to prevent any influence on the measured spectra and dynamics of the absorption lines of ambient water vapor.

Results and Discussion

Linear Spectra. NMA is dominantly present in the trans conformation[10,13,16,20] meaning that the C═O and N−H groups reside on the opposite sides of C−N bond of the NMA molecule. As a result, NMA aggregates can form chainlike structures in which the C═O group of each NMA molecule is hydrogen-bonded to the N−H group of the next NMA molecule in the chain. A solution of NMA in CCl_4 thus consists of chain-wise arranged oligomers of different sizes. Information on the size distribution of these NMA oligomers can be obtained from the linear vibrational absorption spectra of solutions of NMA in CCl_4 of different concentrations. Figure 2 shows two linear spectra of two extreme concentrations of 10 mM (solid black line) and 5 M (dashed black line) solutions of NMA in CCl_4.

The spectra are clearly asymmetric suggesting that they consist at least of two sub-bands. The highest concentration spectrum consists of three sub-bands that closely coincide with the three sub-bands that have been observed before for pure NMA.[7] At the lowest concentration the spectrum consists primarily of a single asymmetric band centered at 1690 cm^{-1} with a tail toward lower frequencies. We fitted this spectrum with a function that is a product of two profiles: a Gaussian

TABLE 1: Summary of the Spectral Positions of Oligomers

species	position (cm^{-1})	fwhm $\Delta\nu$ (cm^{-1})
monomers	1690	~26
dimers	1670	~24
trimers	1655	~19
tetramers	1640	~26

and a Lorentzian with an 80% contribution of the Lorentzian function.[21] This function approximates a voigt profile and allows for a description of the asymmetry of the observed line shape. We used this latter band in combination with the three sub-bands observed at the highest concentration in a global fit of all seven spectra. In this fit the position and spectral widths of the sub-bands are kept constant throughout the concentrations and only the amplitudes have been varied. A separate fit at each concentration showed that the frequency shifts of the four sub-bands for all concentrations are small (<3 cm^{-1}) with respect to the separation between the sub-bands (~15 cm^{-1}) and thus can be neglected. Similarly, the widths of the fitted sub-bands at each concentration are very similar and differ only by ~4 cm^{-1} with respect to the average width of ~24 cm^{-1}. Therefore, the spectra at all concentrations can be desribed with the same 4 sub-bands. The fitted central frequencies of the sub-bands and their spectral widths are summarized in Table 1. The fitted bands used to reconstruct the linear spectra are shown in Figure 2 (thin lines).

In agreement with previous experimental and theoretical studies we assign the four sub-bands to monomers, dimers, trimers, and tetramers.[3,7,11] The absolute positions of the bands differ somewhat between the different studies because different solvents and molecular dynamics algorithms have been used. The fitted central frequencies of the bands correspond well to those found in QCE (quantum cluster equilibrium) simulations[17] and a 2D spectroscopy study on pure NMA.[5]

The precise assignment of the 1640- and 1655-cm^{-1} sub-bands is a topic of debate. Krimm at al.,[4] based on the polarization resolved Raman spectroscopy, showed that for neat NMA the presence of the two sub-bands may be the result of a frequency splitting (so-called noncoincidence effect, NCE) within one sub-band due to transition dipole coupling between the NMA molecules involved in an oligomer. For the present study the precise assignment of the bands at 1640 and 1655 cm^{-1} is not so relevant; what is important is that both bands represent trimers and larger oligomers.

The fit yields the amplitudes of the sub-band at each concentration. By assumption that the cross-section per NMA are the same for each sub-band, we can thus estimate the relative amount of each species at all concentrations. As shown in Figure 3, the monomers are mostly abundant at the lowest concentration (1:1000), accounting for almost 90% of all NMA present. This distribution however changes quickly with increasing concentration, and at a concentration of 50 mM all species are almost equally abundant. At the highest concentration of 5 M (1:1), the monomers are no longer observable. The resemblance between our spectrum at the highest concentration and the spectrum reported by Huang[7] for pure NMA shows that for a 1:1 solution of NMA in CCl_4 the oligomer distribution is similar to that of pure NMA. However, here it should be noted that the most red-shifted band not only contains the NMA tetramers but all oligomers consisting of four and more NMA molecules.

The distribution of NMA oligomers is very sensitive to the temperature. Figure 4 shows a linear spectrum of 50 mM NMA solution at three different temperatures. Upon increasing the temperature, the hydrogen bonds between the NMA molecules

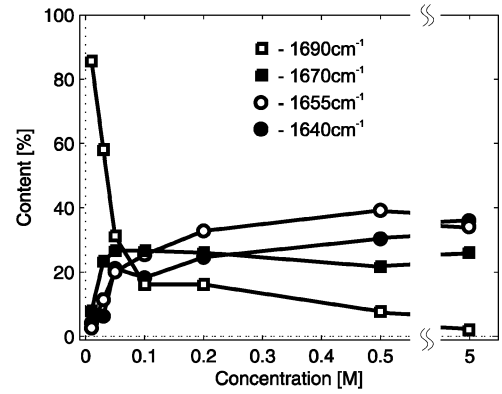

Figure 3. Contribution of the different NMA aggregate sizes to the absorption spectra measured at different concentrations of NMA in CCl_4. Closed circles, 1640 cm^{-1} (≥tetramers); open circles, 1655 cm^{-1} (trimers); closed squares, 1670 cm^{-1} (dimers); open squares, 1690 cm^{-1} (monomers).

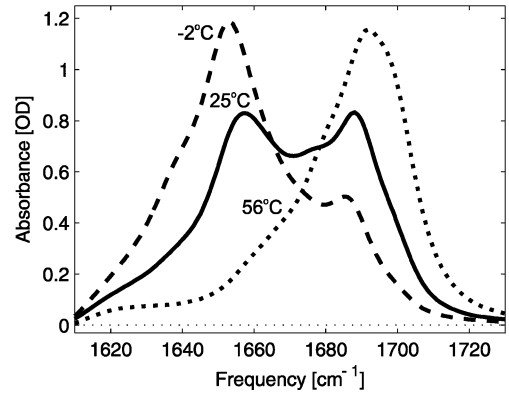

Figure 4. Linear absorption spectra of a solution of 50 mM NMA in CCl_4 (1:200) at three different temperatures.

becomes weaker and break, causing almost all of the oligomers to dissociate into monomers at about 56 °C. This sensitivity of the NMA oligomer size on temperature should be accounted for in the interpretation of the pump−probe data, as we will discuss in the following.

Vibrational Energy Relaxation. ***Exciting the Amide I Mode.*** Figure 5 shows the transient spectral response in the frequency region of the AI and AII modes at different delays after excitation of the AI mode. The most prominent changes are observed at the mode that is being pumped, i.e., the AI mode. At early delays the AI spectrum shows the characteristic transient spectral shape of an excited anharmonic vibration with a negative signal at frequencies around 1660 cm^{-1} originating from the bleaching of the $\upsilon = 0 \rightarrow 1$ transition and a positive signal around 1625 cm^{-1} due to the induced $\upsilon = 1 \rightarrow 2$ transition absorption from the $\upsilon = 1$ excited state. With increasing delay time these signals decay and the shape of the transient spectrum invert. After a few tens of picoseconds we observe a positive signal on the blue side of the AI absorption band and a negative signal on the red side of this band. This shape of the transient spectrum implies a blue shift of the absorption band of the AI mode and forms a characteristic signature of an increase in sample temperature. The blue shift of the absorption band reflects the weakening of the hydrogen bonds, caused by the eventual relaxation and dissipation of the vibrational excitation of the AI mode into heat. At late delays (>40 ps) we observe an additional small change of the transient spectrum: both the negative signal around 1650 cm^{-1} and the positive signal between 1670 and 1680 cm^{-1} increase somewhat further. In

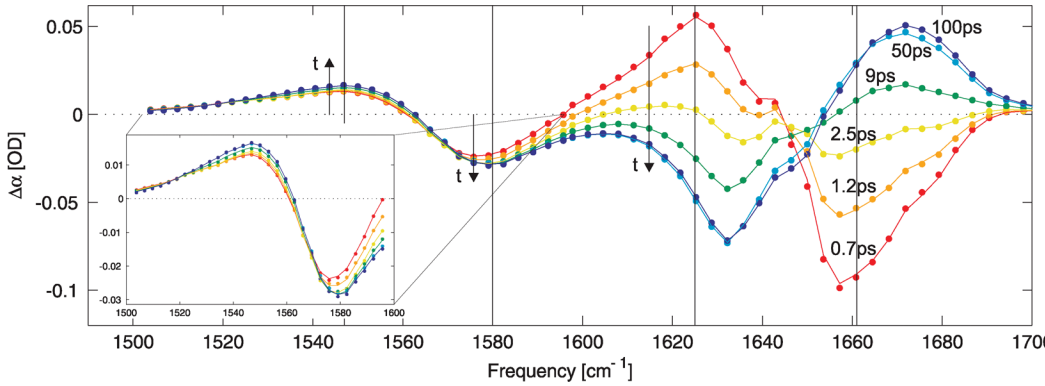

Figure 5. Transient spectra at different delay times following excitation of the amide I mode of NMA for a solution of 5 M NMA in CCl_4.

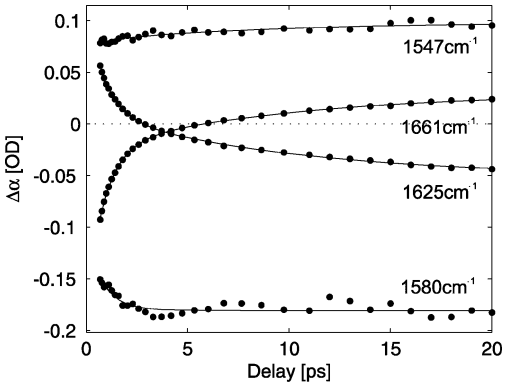

Figure 6. Time traces at four different frequencies corresponding to four thin vertical lines shown in Figure 5. The time traces at 1547 and 1580 cm^{-1} have been multiplied by 6, and offset was added for clarity.

the frequency region between 1640 and 1650 cm^{-1} the transient spectra show a quite irregular structure. This structure is closely connected to the asymmetric shape of the linear absorption spectrum of the AI mode. This spectrum shows a significant shoulder at 1640 cm^{-1} corresponding to the absorption of the tetrameric (and higher order) aggregates (see Figure 2, left spectrum). At early delays, the bleaching of the fundamental transition of the tetramers overlaps with the induced 1⟶2 absorptions of the smaller oligomers and monomers, leading to an irregular structure. At later delay times, the heating of the sample results in a decrease of the concentration of tetramers and an increase of the concentrations of smaller oligomers and monomers. Again the signals of these two contributions overlap and produce an irregular structure of the transient spectrum.

The frequency region near the AII mode shows a very different response after excitation of the AI mode. At early delays, we observe a negative signal at the blue side of the spectrum and a positive signal at the red side. Since the pump spectrum has been tuned to excite only the AI mode, this signal cannot be due to direct excitation of the AII mode. With increasing delay we observe a slight increase of both the negative and positive signals. The signal at late delay times again corresponds to the effect of an increase in temperature, now on the absorption spectrum of the AII mode. For this mode, a temperature increase results in a red-shift of the absorption spectrum, which in the transient spectrum corresponds to a negative absorption change in the blue wing and a positive absorption change in the red wing of the absorption spectrum.

In Figure 6 we present delay traces (dots representing the data points) taken at four frequencies marked in Figure 5 with vertical lines. These frequencies correspond to the centers of the negative and positive parts of the signal for the AI and AII modes. For clarity the two traces of the AII mode were scaled and an offset was added. It is clear from the data that the dynamics of the two modes are different. The traces corresponding to the AII mode show slow dynamics (∼10 ps), whereas the data for AI show fast dynamics at early delays (∼1 ps) and much slower dynamics at later delays (∼10 ps).

Exciting the Amide II Mode. In Figure 7 we show the transient spectral response of both the AI and AII modes after excitation of the AII mode. At frequencies corresponding to the excited AII mode, we observe a bleaching signal of the fundamental 0⟶1 transition and an induced absorption of the 1⟶2 transition at early delays. This signal appears to shift toward higher frequencies with increasing delay time. After about 10 ps, the AII spectrum does not change anymore, meaning that the AII mode has reached an equilibrated thermal state. At the AI mode frequencies, we observe a small signal at early delays (<1 ps) with a shape similar to the spectral shape observed at 2.5 ps in case the AI mode was excited (see Figure 5). The latter signal is followed by the ingrowth of the thermalization signal. Similarly to the case when we pumped the AI mode, we again observe minor spectral changes at later delays in the center and blue side of the AI mode spectrum. No spectral changes at late delays are visible for AII mode.

Figure 8 presents delay traces at four frequencies marked with thin, black vertical lines in Figure 7. The two traces corresponding to the AI mode show a steady ingrowth in time and are very much alike. The traces corresponding to the AII mode show much faster dynamics at early delays. At later delays (>4 ps) the dynamics become much slower.

Interpretation. After excitation of the $v = 1$ state of the AI mode, the bleaching of the 0⟶1 transition and the induced absorption of the 1⟶2 transition of the AI mode rapidly decay with a time constant of ∼1 ps (Figure 6). This rapid decay is followed by a much slower rise of a spectral signature that corresponds to a thermal difference spectrum. Hence, the vibrational relaxation of the $v = 1$ state of the AI mode does not directly lead to a heating effect. This heating effect is delayed, indicating that the excitation energy resides in a nonthermal intermediate state before thermalization occurs. The thermal difference spectrum shows a slow further evolution at time scales >40 ps.

After excitation of the AI mode, the AII mode directly shows a response that has the signature of an anharmonic shift. Because of the excitation of the AI mode, the frequency of the (unexcited) AII mode decreases, leading directly to an increased absorption in the red wing and a bleaching in the blue wing of the AII mode. These transmission changes do not rise with the vibrational lifetime of the AI mode, indicating that the vibra-

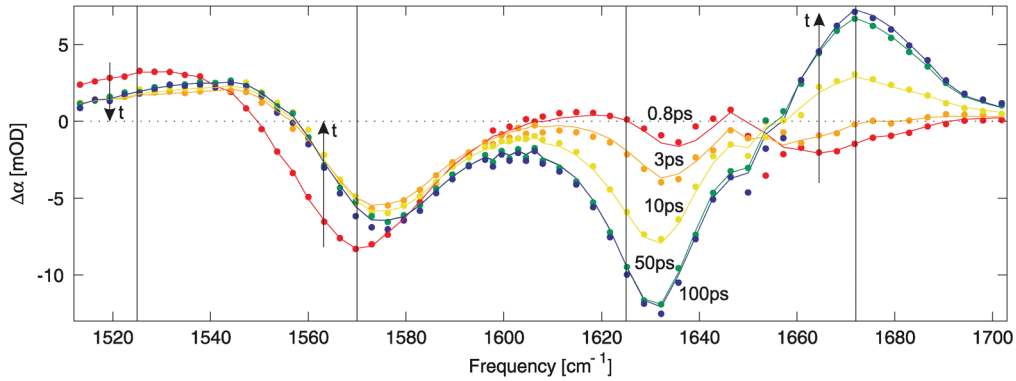

Figure 7. Transient spectra at different delay times following excitation of the amide II mode of NMA for a solution of 5 M NMA in CCl_4.

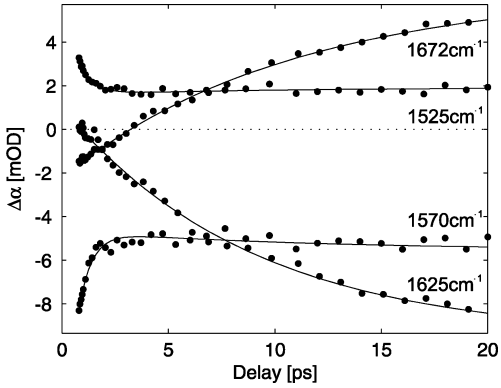

Figure 8. Time traces at four different frequencies corresponding to four thin vertical lines shown in Figure 7.

tional relaxation of the AI mode does not involve energy transfer to the AII mode. At later times, the transient spectrum of the AII mode shows a small increase with the same time constant that is observed for the rise of the thermal difference spectrum in the frequency region of the AI mode.

On the basis of these observations we model our data using a four state consecutive model. Each state has an associated distinct spectrum, and the time evolution of these spectra is described with rates k_1, k_2, and k_3. The occupation of each of the states in time is described by a set of rate equations

$$\frac{d}{dt}\begin{pmatrix} N_1(t) \\ N_2(t) \\ N_3(t) \\ N_4(t) \end{pmatrix} = \begin{bmatrix} -k_1 & 0 & 0 & 0 \\ k_1 & -k_2 & 0 & 0 \\ 0 & k_2 & -k_3 & 0 \\ 0 & 0 & k_3 & 0 \end{bmatrix} \begin{pmatrix} N_1(t) \\ N_2(t) \\ N_3(t) \\ N_4(t) \end{pmatrix} \quad (3)$$

These rate equations are solved using methods described elsewhere.[22] The transient spectra at all delay times are the sum of the time-dependent populations times the associated spectra

$$\Delta\alpha(t,\nu) = \sum_n N_n(t)\sigma_n(\nu) \quad (4)$$

The fitted lifetimes for the consecutive states are shown in Table 2.

The results of the fits are represented as lines in Figure 5 and Figure 6. From the fits we extracted the spectra associated with the different states, as shown in Figure 9.

The black line in Figure 9 is the transient spectrum associated with the first level, i.e., the excited $v = 1$ state of AI. This spectrum shows the bleaching of the 0→1 transition and the induced absorption of the 1→2 transition. In the frequency region of the AII mode this spectrum shows an increased absorption in the red wing and a bleaching in the blue wing. These spectral changes show that the excitation of the AI mode leads to a direct anharmonic red shift of the frequency of the AII mode. The red side of the induced 1→2 transition of the AI model overlaps with the blue wing of the AII mode. As a result, the dynamics at the frequencies around 1580 cm^{-1} (Figure 6) are quite complicated.

TABLE 2: Summary of the Dynamic Parameters of 5 M NMA in CCl_4

excited	probed	T_1 (ps)	T_2 (ps)	T_3 (ps)	τ_r (ps)
AI	AI/AII	0.85 ± 0.1	10 ± 1	~85	~6
AII	AI/AII	0.6 ± 0.1	9 ± 1	~40	~7
AI and AII	AI	1.1 ± 0.1	12 ± 1		

The $v = 1$ state of the AI mode relaxes with $T_1 = 0.85 \pm 0.1$ ps to a nonthermal intermediate state with the spectrum represented by the red line. This spectrum shows very little response in the frequency region of the AI mode, meaning that the absorption spectrum of the AI mode starting from the nonthermal intermediate state is very similar to the absorption spectrum of the AI mode before the excitation. In the frequency region of the AII mode, the transient spectrum of the nonthermal intermediate state is quite similar to that associated with the $v = 1$ mode of AI.

The nonthermal intermediate state relaxes with $T_2 = 10 \pm 1$ ps to the third level that corresponds to a local hot state. In the frequency region of the AI mode, an increase in temperature leads to a blue shift of the absorption spectrum, corresponding to an absorption decrease in the red wing of the AI absorption spectrum and an increase in the blue wing of this spectrum. For the AII mode an increase in temperature results in a red shift, and the associated transient spectrum thus shows an increased absorption in the red wing and a decreased absorption in the blue wing of the AII absorption band. The transition from the nonthermal intermediate state to the local hot state leads to a small increase of the induced absorption in the red wing of the AII mode. This increase shows that the heating effect induces a somewhat larger redshift of the AII mode than the anharmonic coupling with the AI mode and the nonthermal intermediate state. The local hot level relaxes with $T_3 = 85 \pm 10$ ps to the final fully equilibrated state of which the transient spectrum is represented by the green line. This complete equilibration only leads to observable spectral changes in the frequency region of the AI mode.

The data are very well modeled with a frequency independent T_1. This shows that there is no significant variation of the excited state lifetime over the different sub-bands that correspond to

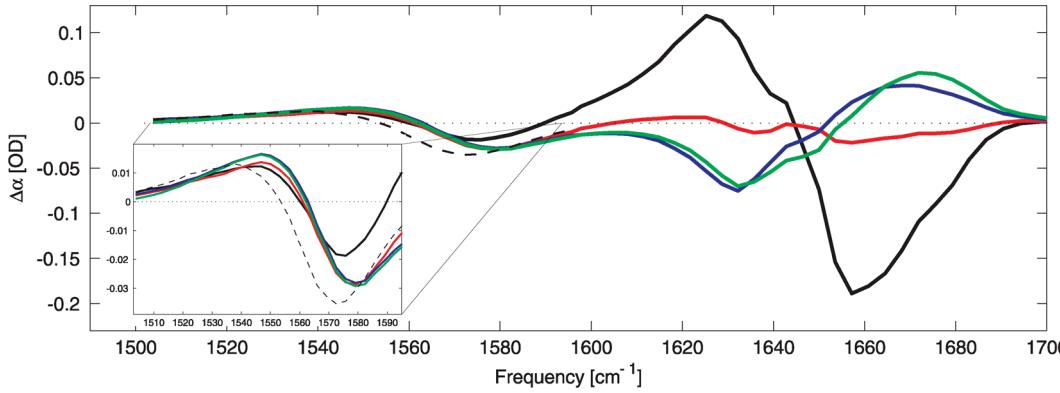

Figure 9. Extracted transient spectra corresponding to the four different states reached in the excitation and vibrational relaxation of the amide I vibration of NMA. For comparison the transient spectrum directly following excitation of the amide II mode is shown (dashed black line).

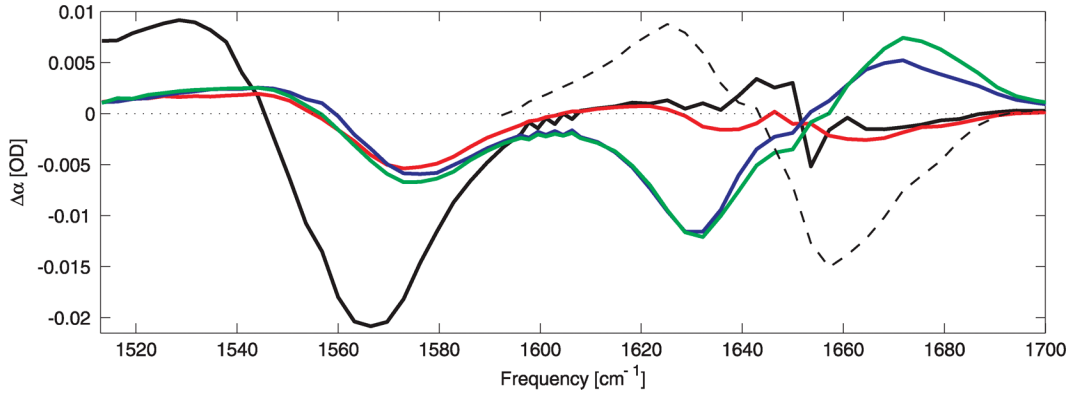

Figure 10. Extracted transient spectra corresponding to the four different states reached in the excitation and vibrational relaxation of the amide II vibration of NMA. For comparison the transient spectrum directly following excitation of the amide I mode is shown (dashed black line).

different oligomers. The T_1 relaxation is thus a local effect, governed primarily by the local hydrogen bond.

Excitation of the $v = 1$ state of the AII mode leads to a similar relaxation scheme as is observed after excitation of the AI mode. The extracted lifetimes are shown in Table 2. The result of the fit is shown with the solid lines in Figures 7 and 8. The transient spectra that describe the spectral dynamics are illustrated in Figure 10. The black line represents the transient spectrum associated with the excitation of the $v = 1$ mode of AII. This spectrum shows the bleaching of the 0→1 transition and the induced absorption of the 1→2 transition. It is noteworthy that the frequency difference between these two transitions is substantially larger (by ~10 cm^{-1}) than the difference between the positive and negative signals originating from the anharmonic shift of the AII absorption frequency induced by the excitation of the AI mode (see inset in Figure 9). This notion confirms that the transient spectral shapes observed in Figure 9 in the frequency region of the AII mode are not due to energy transfer from the excited $v = 1$ state of the AI mode to the $v = 1$ state of the AII mode.

The transient spectrum associated with the $v = 1$ state of the AI mode does not show a strong response in the frequency region of the AI mode. The transient spectrum (black line) indicates the presence of an anharmonic red shift of the AI absorption frequency upon excitation of the AII mode.

The $v = 1$ state of the AII mode relaxes with $T_1 = 0.65 \pm 0.1$ ps to a nonthermal intermediate state. The spectrum associated with this state (red line in Figure 10) is similar to the transient spectrum observed for the nonthermal intermediate state in the relaxation of the AI mode. This suggests that the nonthermal intermediate state is composed of the same vibrational excitations in both cases. The nonthermal intermediate state relaxes to the local hot state with $T_2 = 9.5 \pm 1$ ps. This time constant is quite similar to the relaxation time constant of the nonthermal intermediate state in the relaxation of the AI mode, supporting the idea that the nonthermal intermediate state may be the same in both cases. The local hot state relaxes to a fully equilibrated state with $T_3 = \sim 40$ ps. The transient spectrum of the local hot state and fully equilibrated state are also quite similar to what was observed after excitation of the AI mode. The transition to the fully equilibrated state again only leads to changes in the spectrum in the frequency region of the AI mode.

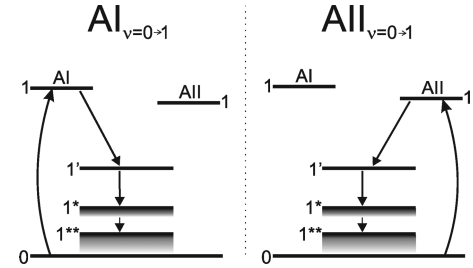

Figure 11. Energy level diagram and vibrational energy relaxation pathways of NMA upon excitation of the amide I mode (left panel) and excitation of the amide II mode (right panel).

Figure 11 summarizes the observed relaxation pathways upon selective excitation of either the AI or AII mode.

Discussion. The AI mode shows much stronger changes in its transient spectral response during the vibrational relaxation than the AII mode. This stronger response can be explained from the fact that the frequency shifts of the AI mode at different stages of the relaxation have opposite signs. The excitation of the $v = 1$ state leads to a red-shifted 1→2 induced absorption of the AI mode, whereas the relaxation to the local hot state

and the final equilibrated state lead to a blue shift of the absorption of this mode. For the AII mode, heating and thus the final thermalization process of the relaxation results in a red shift of the absorption spectrum.[5,7,17] Hence, for this mode, both the transient spectral response directly after the excitation of its $v = 1$ state and the final response resulting from the thermalization are formed by red shifts. In addition, the nonthermal intermediate state also induces an anharmonic red shift of the absorption spectrum of the AII mode. Hence, at all stages the transient response of the AII mode is similar, making the changes in the transient spectral response during the relaxation relatively small. Nevertheless, there are changes in the spectral response during the relaxation as the transient spectral response of the 1→2 induced absorption of the AII mode is not the same as the change in spectral response resulting from the heating of the sample.

We observe quite similar relaxation mechanisms following excitation of the AI and the AII mode. In neither case we observe direct energy transfer between the AI and AII modes. The observed spectral signatures at early delays indicate the presence of an anharmonic coupling between the excited and the unexcited modes, in both cases leading to a red shift of the absorption spectrum. One possible reason for the lack of any energy transfer between AI and AII modes could be the formation of NMA clusters. The presence of hydrogen bonds in these clusters strongly increases the density of potentially accepting vibrational states. Hence, the relaxation of the excited $v = 1$ states to combination tones of lower-energy intra- and intermolecular vibration can be very efficient, thus preventing the energy transfer between the $v = 1$ states of the AI and AII modes.

There have been a few earlier experimental[6,8] and theoretical[14,15,23] studies of the energy dynamics of the amide modes of NMA. DeFlores et al.[8] reported the occurrence of rapid vibrational equilibration between the AI and AII modes for hydrogen bonded NMA (NMA in D_2O and in DMSO). These results were confirmed by results of molecular dynamics simulations (MD),[15] which found the population exchange time between the modes to be ∼0.5 ps. Interestingly, in two other MD simulation studies no energy transfer between the $v = 1$ states of the AI and AII modes was found. Instead, independently of which mode is excited (AI or AII), the vibrational energy is found to be directly transferred to lower frequency modes and then to the solvating bath.[14,23] Clearly, these results are very much in line with the present experimental data.

The transient spectra of Figure 9 and Figure 10 contain some clues as to the nature of the nonthermal intermediate state. The fact that the occupation of this state leads to significant spectral changes in the frequency region of the AII mode suggests that this state must comprise excitations of vibrational modes that are quite efficiently anharmonically coupled to the AII mode. Similarly, the fact that the intermediate state has less effect on the AI mode suggests that this mode is of quite different character. The contributions of the different local modes of NMA to the amide normal modes have recently been determined with potential energy distribution calculations (PED)[3,4,14,18] (both for isolated NMA and hydrogen bonded NMA). Since the AI mode is dominated by the C═O stretch vibration (∼80%),[14,16,18,24] the nonthermal intermediate state likely does not contain much of this vibrational character. We can thus exclude the amide IV (∼615 − 630 cm^{-1}) mode containing about 40% of C═O rocking mode character and the amide VI (∼605 − 630 cm^{-1}) mode containing about 80% of C═O out-of-plane bending mode character. The AII mode is of strongly mixed character, and thus there are quite a few low-frequency modes (AIII, AV−AVII) that can efficiently couple to it. It is therefore likely that the nonthermal intermediate state represents excitations in modes other than the AIV and the AVI modes. The most feasible is the AIII mode, which as shown in the MD simulations[14] can act as a vibrational energy acceptor for either excited AI or AII modes.

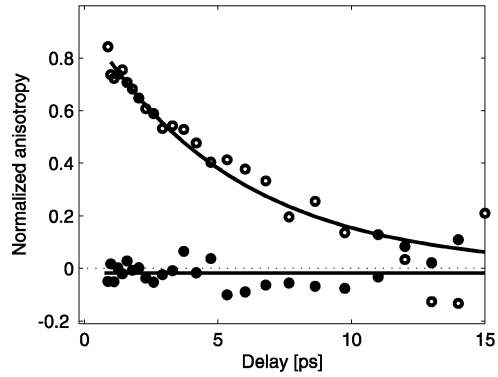

Figure 12. Anisotropy decays for the amide I mode (open circles) and amide II mode (black circles) following excitation of the amide I mode of NMA for a solution of 5 M NMA in CCl_4.

The second time scale T_2 of ∼10 ps found in the relaxation processes is assigned to the thermal equilibration time between the nonthermal intermediate state (low-frequency modes excited) and the directly surrounding solvent molecules. A similar value of ∼9 ps was found for the equilibration time between an excited dye molecule and tetrachloroethylene,[25] which is a similar to the carbon tetrachloride, which is used as a solvent in the present study. In the present study we observe that the thermalization is not complete after the relaxation process with T_2 of ∼10 ps. We observe an additional equilibration step with time constant T_3 representing the transition from a local hot state to the truly thermally equilibrated state of the molecule. In this state the distribution of NMA clusters has completely adapted to the increased temperature in the focus.

The final equilibration process is observed to have a much stronger influence on the absorption spectrum of the AI mode than on the AII mode. This observation can be explained from the influence of the hydrogen-bond interaction on the spectrum of the two amide modes. The NMA molecules are hydrogen bonded via their N−H (hydrogen-bond donor) and C═O (hydrogen-bond acceptor) groups. A change in the strength of the hydrogen-bond interaction will thus most strongly influence the spectral response of the amide vibrations that possess strong N−H stretch or C═O stretch vibrational character. The AI mode possesses very strong C═O stretch vibrational character, and thus the weakening of this bond, as will occur in both the second and third relaxation process, will have a strong influence on the absorption spectrum of this mode. In contrast, the AII modes possesses neither strong N−H stretch nor C═O stretch vibrational character, thereby making this mode much less susceptible to changes in the hydrogen-bond interaction.

Anisotropy Data. The polarization resolved pump−probe experiments were used to construct the anisotropy parameter $R(t, \nu)$. Figure 12 presents time traces of the anisotropy at the central frequency of the AI mode (open circles) and the central frequency of the AII mode (closed circles), both after excitation of the AI mode. The anisotropy of the AI mode thus reflects the reorientation of the AI transition dipole moment. The anisotropy of the AII mode reflects the relative angle between the transition dipole moment orientations of the two modes. In

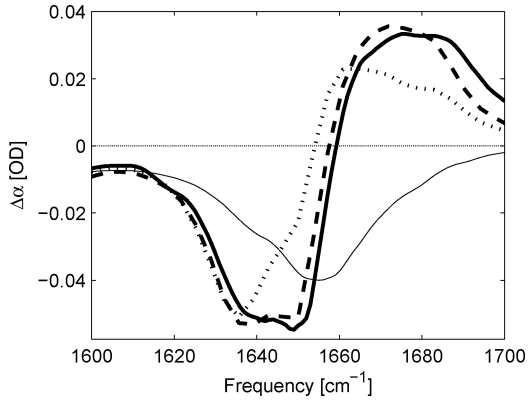

Figure 13. Spectra of the local hot state (dotted line) and final equilibrated state (dashed line) of NMA measured after broad-band infrared excitation of the amide I and amide II vibrations of NMA for a solution of 5 M NMA in CCl_4. The thick solid line represents the differential linear absorption spectrum obtained by subtracting linear absorption spectra at different temperatures. The thin solid line represents the linear absorption spectrum at 300 K.

case the AII mode is excited we observe the same anisotropy dynamics for the excited and unexcited mode (not shown).

The anisotropy of the excited AI mode decays with a time constant of $\tau_r = \sim 6$ ps. This time constant represents the reorientation time of this mode, averaged over all oligomers. This reorientation time is relatively long for a weakly interacting solute−solvent system such as NMA−CCl_4. However, the NMA molecules are hydrogen-bonded, which will strongly slow down their reorientation. A similar value of ~6 ps has been reported previously for NMAD (deuterated NMA) in D_2O.[26]

The anisotropy of the AII remains constant around $R(t, \nu) = 0$. The anisotropy shows the following dependence on the relative angle θ between the transition dipole moments of the excited and probed mode

$$R(t, \nu) = \frac{1}{5}(3\cos(\theta)^2 - 1) \tag{5}$$

From eq 5 it follows that the observed AII anisotropy can be zero only at all delay times for θ very close to the "magic angle" (54.7°). The observed anisotropy traces thus imply that the average angle between the transition dipole moment orientations of AI and AII amounts to 56 ± 3°. This angle agrees with the angle found previously for both bonded and nonbonded NMA.[8] Hence, upon clustering/hydrogen bonding of the NMA molecules the angle between the transition dipole moment orientations of the AI and AII modes does not change, which indicates that the contributions of the different local modes to these amide modes is not strongly affected by the presence of hydrogen bonds between the NMA molecules.

Thermalization Dynamics. To investigate the thermalization processes following vibrational relaxation in more detail we performed a few additional experiments. In one experiment, we excited both the AI and AII modes with an intense broadband, high-energy pump pulse. We probe the AI mode, as this mode shows the strongest effects of the thermalization dynamics. As in Figure 5, we observe a slow signal ingrowth in the center and blue wing of the AI absorption band in the delay time range between 30 and 100 ps. We fit the data with the same 4 level consecutive relaxation model that we used in the modeling of the 2D experiments. The two final extracted spectra are shown in Figure 13. For comparison we also include a differential linear spectrum (solid thick line in Figure 13) of the sample measured

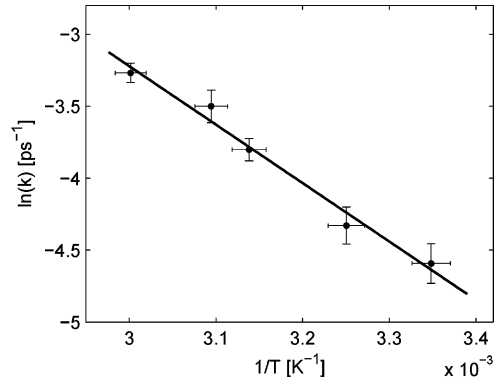

Figure 14. Arrhenius plot of the time scale T_3 of the final relaxation process after broad-band infrared excitation of the amide I and amide II vibrations of NMA for a solution of 5 M NMA in CCl_4.

at two different temperatures. The differential linear spectrum shows a very good correspondence with the final thermal spectrum, thereby confirming that the fourth state in the relaxation model indeed corresponds to a fully thermally equilibrated state. It is known from linear infrared spectroscopic studies that NMA clusters dissociate into smaller sizes upon an increase in temperature. We therefore attribute the change in the spectral response to the dissociation of NMA aggregates $nma_1 \cdots nma_2 \cdots nma_n$ into smaller forms. The positive absorption signal at 1670−1680 cm^{-1} is thus caused by the production of non-hydrogen bonded NMA, and the bleach at ~1650 cm^{-1} reflects the disappearance of NMA dimers, trimers, and larger oligomers.

In a second experiment, we studied the dependence of the thermalization dynamics on the nature of the excited NMA oligomer. In this experiment, we have selectively excited either dimers or tetramers and higher-order clusters with a spectrally narrow pump ($\Delta\nu = \sim 10$ cm^{-1}) centered at 1675 or 1630 cm^{-1}, respectively. In both cases we found the time evolution and the spectral changes to be exactly the same at all times. This observation shows that at the stage of the local hot state the energy is already quite delocalized over different NMA clusters. Hence, the last relaxation process with time constant T_3 does not represent an energy redistribution process but rather a repositioning of the NMA molecules, i.e., the partial dissociation of the NMA aggregates.

In a final experiment, we measured the relaxation dynamics at different initial sample temperatures, again using an intense broadband infrared excitation pulse. We observe that the lifetimes of the excited $v = 1$ and nonthermal intermediate states do not change with temperature. At all temperatures we obtain $T_1 = 1.1 \pm 0.1$ ps and $T_2 = 12 \pm 1$ ps. However, the time constant T_3 of the transition from the local hot state to the final fully equilibrated state is observed to be strongly temperature dependent. These time constants are used to determine the activation energy of the dissociation process, using Arrhenius law

$$\ln(k) = \ln(A) - \frac{E_a}{R}\left(\frac{1}{T}\right) \tag{6}$$

where k is measured dissociation rate, A a pre-exponential factor, R the gas constant, and E_a the activation energy. Figure 14 shows the dependence of the dissociation rate on the temperature. The slope of the fitted linear function gives the activation energy for the dissociation process $E_a = 35 \pm 3$ kJ mol^{-1}.

The activation energy for the dissociation process represents the energy barrier to move two hydrogen-bonded NMA molecules apart and will be similar to the binding energy of the hydrogen bond with which the two NMA molecules are connected. In a strongly interacting solvent the activation energy could be somewhat lower than the binding energy of the hydrogen bond if the dissociation of the hydrogen bond would directly allow new favorable interactions between the NMA molecules and the solvent. However, in a weakly interacting solvent like CCl_4 this effect will be negligible, and thus E_a will be close to the hydrogen bond binding energy. The value of E_a of 35 ± 3 kJ mol^{-1} is in excellent agreement with previously reported values that are obtained from infrared measurements[27] ($\sim$33−38 kJ mol^{-1}) and dielectric measurements[9] (31.5 kJ mol^{-1}). In view of the cooperativity of the hydrogen-bond interaction, the hydrogen-bond binding energy E_H will depend on the size of the oligomer and the position within the NMA oligomer. By use of infrared spectroscopy Herrebout et al.[3] finds average hydrogen-bond binding energies of 31.8, 35.3, and 37.3 kJ mol^{-1} for dimers, trimers, and tetramers, respectively. Very similar values are reported in molecular orbital simulations[11] and molecular dynamics simulations[12] (dimer, 29 kJ mol^{-1}; trimer, 36 kJ mol^{-1}; tetramer, 39 kJ mol^{-1}).

Conclusions

We studied the vibrational absorption spectra and energy relaxation dynamics of NMA aggregates in CCl_4 using linear and two-color femtosecond infrared spectroscopy. We measured infrared spectra over a large concentration range ranging from 10 mM to 5 M. With increasing concentration, the absorption spectrum of the amide I mode of NMA is observed to shift toward lower frequencies, indicating the formation of hydrogen-bond clusters. The spectra at all concentrations can be decomposed into four sub-bands that correspond to NMA clusters of different sizes: monomers (1690 cm^{-1}), dimers (1670 cm^{-1}), trimers (1655 cm^{-1}), and tetramers + higher-order oligomers (1640 cm^{-1}).

We observe similar vibrational relaxation pathways following excitation of the amide I and amide II vibrations. In a first relaxation step, the energy is transferred from the excited $v = 1$ state of either vibrational mode to a nonthermal intermediate state. For the amide I mode this process has a time constant T_1 of 0.85 ± 0.1 ps; for the amide II mode $T_1 = 0.65 \pm 0.1$ ps. We do not observe energy transfer between the amide I and amide II modes. The intermediate state is formed by a combination tone of excited lower-energy vibrational states and appears to be quite similar in character for amide I and amide II excitation as evidenced by the similarity in the effects of the occupation of this state on the absorption spectra of the amide I and amide II modes. In both excitation schemes, the occupation of the intermediate state has a much stronger (anharmonic) effect on the absorption spectrum of the amide II mode than on the absorption spectrum of the amide I mode, which suggests that this state comprises local vibrational modes that are much more strongly coupled to the amide II than to the amide I mode. The intermediate state relaxes in a second process with time constant $T_2 = \sim 10 \pm 1$ ps to a state that can best be denoted as a local hot state. In this state the energy has been equilibrated over the NMA aggregates and the neighboring solvent molecules. In a third and final relaxation process with time constant $T_3 = 40-100$ ps, a full equilibration of the sample in the focus takes place. In this latter process the NMA clusters partly dissociate, thus forming the equilibrium aggregate size distribution that corresponds to the new, higher temperature. The measurement of the rate of this final process reveals the activation energy of the dissociation of the NMA clusters to be $E_a = 35 \pm 3$ kJ mol^{-1}. This energy corresponds to the average binding energy of a hydrogen bond between two NMA molecules.

We also studied the reorientation time of the NMA molecules and the relative orientation of the transition dipole moments of the amide I and amide II modes using polarization-resolved femtosecond pump−probe measurements. We found that the average reorientation time of the NMA molecules equals 6 ps. The relative angle between the transition dipole moment orientations of the amide I and amide II modes is θ (AI, AII) $= 56 \pm 3°$.

Acknowledgment. The work is part of the research program of the Foundation for Fundamental Research on Matter, which is financially supported by the Dutch organization for Scientific Research (NWO). This work has been financially supported by the European Union Marie Curie Program (MEST-CT-2005-021000). The authors would like to thank Hinco Schoenmaker for technical support.

References and Notes

(1) Selkoe, D. *Nature* **2003**, *426*, 900–904.
(2) Liu, Y.; Czarnecki, M. A.; Ozaki, Y. *Appl. Spectrosc.* **1994**, *48*, 1095.
(3) Herrebout, W. A.; Clou, K.; Desseyn, H. O. *J. Phys. Chem. A* **2001**, *105*, 4865.
(4) Chen, X.; Schweitzer-Stenner, R.; Asher, S.; Mirkin, N.; Krimm, S. *J. Phys. Chem.* **1995**, *99*, 3074–3083.
(5) Noda, I.; Liu, Y.; Y., O. *J. Phys. Chem.* **1996**, *100*, 8665–8673.
(6) Rubtsov, I. V.; Wang, J. P.; Hochstrasser, R. M. *J. Phys. Chem. A* **2003**, *107*, 3384–3396.
(7) Huang, H.; Malkov, S.; Coleman, M.; Painter, P. *J. Phys. Chem. A* **2003**, *107*, 7697–7703.
(8) DeFlores, L. P.; Ganim, Z.; Ackley, S. F.; Chung, H. S.; Tokmakoff, A. *J. Phys. Chem. B* **2006**, *110*, 18973–18980.
(9) Omar, M. M. *J. Chem. Soc. Faraday Trans.* **1980**, *76*, 711–716.
(10) Pralat, K.; Jadzyn, J.; Balanicka, S. *J. Phys. Chem.* **1983**, *87*, 1385.
(11) Torii, H.; Tatsumi, T.; Kanazawa, T.; Tasumi, M. *J. Phys. Chem. B* **1997**, *102*, 309–314.
(12) Jiang, X.-N.; Wang, C.-S. *Chem. Phys. Chem.* **2009**, *10*, 3330–3336.
(13) Akiyama, M.; Torii, H. *Spec. Chim. Acta A. Mol. Bio.* **1999**, *56*, 137.
(14) Zhang, Y.; Fujisaki, H.; Straub, J. *J. Phys. Chem. A* **2009**, *113*, 3051–3060.
(15) Bloem, R.; Dijkstra, A.; Jansen, T.; Knoester, J. *J. Chem. Phys.* **2008**, *129*, 55101.
(16) Miyazawa, T.; Shimanouchi, T.; Mizushima, S.-I. *J. Chem. Phys.* **1958**, *29*, 611.
(17) Ludwig, R.; Reis, O.; Winter, R.; Weinhold, F.; Farrar, T. C. *J. Phys. Chem. B* **1998**, *102*, 9312–9318.
(18) Myshakina, N.; Ahmed, Z.; Asher, S. *J. Phys. Chem. B Lett.* **2008**, *112*, 11873–11877.
(19) Graener, H.; Seifert, G.; Laubereau, A. *Chem. Phys.* **1993**, *175*, 193–204.
(20) Köddermann, T.; Ludwig, R. *Phys. Chem. Chem. Phys.* **2004**, *6*, 1867–1873.
(21) Cringus, D.; Yeremenko, S.; Pshenichnikov, M. S.; Wiersma, D. A. *J. Phys. Chem. B* **2004**, *108*, 10376–10387.
(22) Timmer, R. L. A.; Bakker, H. J. *J. Chem. Phys.* **2007**, *126*, 154507.
(23) Gregurick, S.; Chaban, G.; Gerber, R. *J. Phys. Chem. A* **2002**, *106*, 8696–8707.
(24) Mizushima, S.-I.; Simanouti, T.; Nagakura, S.; Kuratani, K.; Tsuboi, M.; Baba, H.; Fujioka, O. *J. Am. Chem. Soc.* **1950**, *72* (8), 3490–3494.
(25) Dahinten, T.; Baier, J.; Seilmeier, A. *Chem. Phys.* **1998**, *232*, 239–245.
(26) Hamm, P.; Lim, M.; Hochstrasser, R. M. *J. Phys. Chem. B* **1998**, *102*, 6123–6138.
(27) Pimental, G. C.; Maclellan, A. L. *The Hydrogen Bond*; Freeman, 1960.

JP107590B